Korean J. Chem. Eng., 36(1), 37-47 (2019)
DOI: 10.1007/s11814-018-0169-7

pISSN: 0256-1115
eISSN: 1975-7220

Facile and simple synthesis of triethylenetetramine-modified mesoporous silica adsorbent for removal of Cd(II)

Atena Abedi*, Hamidreza Ghafouri Taleghani*,†, Mohsen Ghorbani, and Hamed Salimi Kenari***

*Faculty of Chemical Engineering, University of Mazandaran, Babolsar, Iran
**Faculty of Chemical Engineering, Babol Noshirvani University of Technology, Babol, Iran
(*Received 4 April 2018 • accepted 11 October 2018*)

Abstract−Monodispersed porous silica microspheres (SM) were synthesized and further functionalized with amine moieties using triethylenetetramine (TETA) in order to obtain a novel adsorbent for Cd(II) elimination from aqueous media. The morphology, texture and structure of samples were characterized with the aid of Fourier transform infrared spectroscopy (FTIR), X-Ray diffraction (XRD), scanning and transmission electron microscopy (SEM, TEM), energy dispersive spectroscopy (EDS), and N_2 adsorption-desorption. The adsorption efficiency was investigated based on the effect of operational parameters including pH of the solution, the dose of adsorbent, adsorption time, initial concentration of Cd(II) ions and temperature. The equilibrium, kinetics and thermodynamics of Cd(II) adsorption were also studied. The maximum adsorption capacity of amine functionalized silica microspheres (AMSM) for Cd(II) was 35.6 mg g^{-1}. Cd(II) adsorption onto AMSM had highest consistency with Sips and Langmuir isotherms, while adsorption kinetics was best fitted with pseudo-second order model. Thermodynamics of adsorption revealed that Cd(II) adsorption on AMSM was spontaneous, feasible and exothermic with physical interactions and pore diffusion being the dominant mechanisms in the adsorption process. Results confirmed that AMSM adsorbent has the potential to be a suitable candidate for Cd(II) removal from aqueous solutions.

Keywords: Mesoporous, Silica Microspheres, Amine Functionalized, Adsorption, Cd(II) Removal

INTRODUCTION

Cadmium is classified as a highly carcinogen heavy metal with harmful impacts on human health and living organisms [1]. It is commonly discharged into water sources from metallurgical alloying, ceramics, pigment industries, alkali batteries, and plastics wastewaters [2]. The weak response of cells and comparatively long half-life of 10 to 30 years for Cd(II) ions in living organs indicates that it is highly non-biodegradable and toxic. Cd(II) exposure causes renal disorder, osteoporosis, neurological malfunction, cancers, genetic toxicity, endocrine damage and fertility problems for human being [3,4]. Therefore, it is highly important to develop procedures for the treatment of cadmium-contaminated industrial wastewater before being discharged into the environment.

Adsorption technique is one of the most promising separation methods commonly applied for the removal of pollutants including heavy metals, dyes and many organic contaminants from aqueous solution [5]. Adsorption is preferred over other conventional purification techniques due to simplicity, low expenditure, high efficiency and possible regeneration of adsorbents [6,7]. A variety of natural organic and mineral adsorbents, such as red mud [8], rice husk [9], biochar [10], tannin [11] and activated carbon [12], were applied to eliminate cadmium ions.

Luo et al. [13] reported an adsorption capacity of 41.6 mg g^{-1} for cadmium removal using MnO_2 functionalized MWCNTs [13]. Sari and Tuzen [14] investigated the Cd(II) removal from aqueous solution and waste water by raw kaolinite and manganese oxide (MnO_2)-modified kaolinite (MnO-Kaol). The result showed that the adsorption capacity of raw and modified kaolinite was 14.11 and 36.47 mg g^{-1} respectively [14]. Liang et al. [15] investigated the removal of cadmium on alumina decorated MWCNTs and found an adsorption capacity of 27.21 mg g^{-1} [15]. Ruthiraan et al. [1] using functioned multiwall carbon nanotubes and magnetic biochar for Cd removal from aqueous solution found an adsorption capacity of 83.3 mg g^{-1} and 62.5 mg g^{-1}, respectively [1]. Xue et al. [16]. synthesis graphene oxide nanosheets for the removal of Cd(II) ions from acidic aqueous solutions. They found that the calculated maximum adsorption capacity value for Cd(II) was 44.64 mg g^{-1} at pH 4.00 [16]. Yu et al. [17] prepared poly(maleic acid)-grafted cross-linked chitosan microspheres for Cd(II) adsorption. They reported that the maximum adsorption capacity was 39.2 mg g^{-1} [17].

Mesoporous silica is considered a superior adsorbent for heavy metal removal, fulfilling most of the desired criteria of an outstanding adsorbent with superior specific surface area, narrow pore-size distributions and controlled pore sizes [18]. In addition, the affinity and selectivity towards target heavy metals in these structures can easily be improved by introducing suitable functional groups to the surface, which creates new available adsorption sites [19]. In research performed by Lin and coworkers [20], mesoporous silica was successfully functionalized with thiol groups and its performance for heavy metal removal was investigated. Liu et al. [21] reported the synthesis of thiol and amine treated mesoporous silica and indicated that amine treated samples had exceptionally higher adsorption efficacy toward copper ions. Najafi and coworkers [22]

†To whom correspondence should be addressed.
E-mail: H.Taleghani@umz.ac.ir

also demonstrated the improved performance of silica nano hollow spheres and silica gel for the removal of some heavy metals after amine functionalization.

In this study we prepared mesoporous silica microspheres (SM) and amine functionalized silica microspheres (AMSM) using a versatile method and investigated the structural, textural and morphological characteristics of the sample. The AMSM sample was then applied for the adsorption of Cd(II) ions. The effects of operational parameters on adsorption efficiency, equilibrium, kinetic and thermodynamic aspects of Cd(II) adsorption were investigated.

EXPERIMENTAL

1. Reagents

Dodecylamine, tetraethyleorthosilicate (TEOS), Triethylenetetramine (TETA), Ethanol (99%), all in analytical grade, were purchased from Merck and used without further purification. Distilled water was used as the solvent.

2. Synthesis of Silica Microspheres (SM)

In the preparation of SM samples, dodecylamine and TEOS were used as the templating agent and the silica source, respectively. A solution of ethanol (160 mL) and distilled water (100 mL) was prepared into which 1.44 g of dodecylamine was dissolved followed by dropwise addition of 10 mL TEOS. After 4 h, the precipitate was filtered, thoroughly washed with water and ethanol and then dried at 80 °C for 6 h. Finally, the templates were removed from the samples by calcination at 600 °C for 4 h [23].

3. Preparation of Amine Functionalized Silica Microspheres (AMSM)

The AMSM samples were prepared by TETA, as the organic amine. 2.82 g of amine precursor was dissolved in 20 mL of ethanol and stirred for 0.5 h, then 0.2 g of monodispersed porous silica, pre-treated at 80 °C in a vacuum condition, were added. After 30 min, the sample was dried at 70 °C for 16 h and another 1 h at 80 °C for the complete evaporation of ethanol [24].

4. Characterization Techniques

FT-IR spectra of SM and AMSM samples were taken on a Bruker-Tensor 27 IR spectroscope at 400 to 4,000 cm^{-1} and resolution of 2 cm^{-1}. Low angle XRD patterns of samples were collected using Panalytical X'pert Pro equipment within the 2θ range of 0.5° to 8°. Morphology of SM and AMSM samples was monitored using MIRA3 TESCAN field emission scanning electron microscopy operating at a voltage of 5 KV with an EDS analyzer (SAMx company, France) used for elemental analysis. TEM graphs were taken using 80 kV Zeiss-EM10C transmission electron microscopy. The N_2 adsorption/desorption isotherms for the samples were measured on a BELSORP Mini (II), instrument. The textural properties of samples including specific surface area, pore volume and pore diameter distribution were calculated using the Brunauer-Emmett-Teller and Barrett-Joyner-Halenda (BJH) algorithms. Cd(II) concentration was measured using a Perkin Elmer atomic emission spectrometer.

5. Adsorption Experiments

The adsorption performance of AMSM adsorbent for Cd(II) ion removal was evaluated through batch adsorption experiments with variation of operational parameters including effluent pH, initial concentration of Cd(II) ions, the amount of the adsorbent, contact time and temperature. 1,000 mg L^{-1} stock solution of Cd(II) ions was prepared by dissolving the desired amount of $Cd((NO_3)_2 \cdot 4H_2O$; the required concentrations of Cd(II) were further prepared by diluting the stock solution. Cadmium concentrations were analyzed with a VISTA-PRO (Varian, Australia) CCD simultaneous inductively coupled plasma optical emission spectroscopy (ICP-OES) system with a detection limit of 4.0×10^{-5} mgL^{-1} for cadmium. Each sample was measured in triplicate, and the average results are reported.

The effect of pH on Cd(II) removal efficiency was evaluated by mixing 40 mg of adsorbent with 15 mL solution of Cd(II) (50 mg L^{-1}) with different pH values adjusted at 2,3,4 and 5. To evaluate the effects of adsorption time (30-210 min with 30 min time intervals), adsorbent dosage (5-60 mg), initial Cd(II) concentration (5-100 mg L^{-1}) and temperature (298, 308 and 318 K), 40 mg of AMSM adsorbent was added to a series of 15 mL Cd(II) solutions prepared for each parameter, shaken at 250 rpm for 180 min. The adsorbents were then simply filtered and the remaining concentration of Cd(II) ions in the solution was calculated by ICP. Triplicate runs of each experiment were performed and the mean values were reported. The removal efficiency and adsorption capacity of AMSM adsorbent were calculated as follows:

$$\text{Adsorption Efficiency}\,(\%) = \frac{C_0 - C_e}{C_0} \times 100 \quad (1)$$

$$q_e = \frac{V(C_0 - C_e)}{m} \quad (2)$$

In which q_e is equilibrium adsorption capacity of AMSM toward Cd(II) (mg g^{-1}), C_0 and C_e are the initial and equilibrium concentration of Cd(II) ions in the solution (mg L^{-1}), respectively, V is the volume of Cd(II) ions solution (L) and m is the weight of adsorbent (g).

RESULTS AND DISCUSSION

1. Characterization of SM and AMSM

1-1. FTIR Spectroscopy

The FTIR spectra of SM and AMSM samples are illustrated in

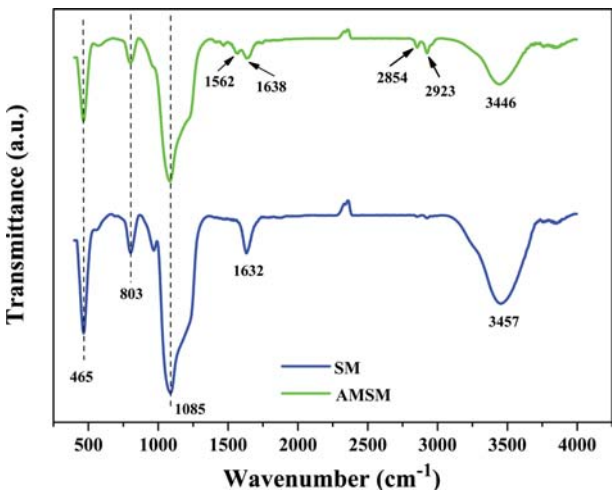

Fig. 1. FTIR spectra of SM and AMSM samples.

Fig. 1. It is evident that both SM and AMSM samples exhibit a rather broad FTIR absorption peak at around 3,200-3,800 cm^{-1} wavenumber attributed to the O-H stretching modes of silanol groups in the inorganic framework of silica and also to the capillary pore water or surface absorbed water. It can be seen that the introduction of amine groups on SM resulted in an intensity reduction and a slight wavenumber shift in this region, which certifies that a strong interaction occurred between the surface hydroxyl and amine groups. In addition, the peaks at 2,923, 2,854 cm^{-1} can be assigned to C-H stretching modes in the hydrocarbon chain of dodecylamine. The peaks at 465 and 803 cm^{-1} are ascribed to the bending and symmetric stretching vibrations of siloxane (Si-O-Si) groups,

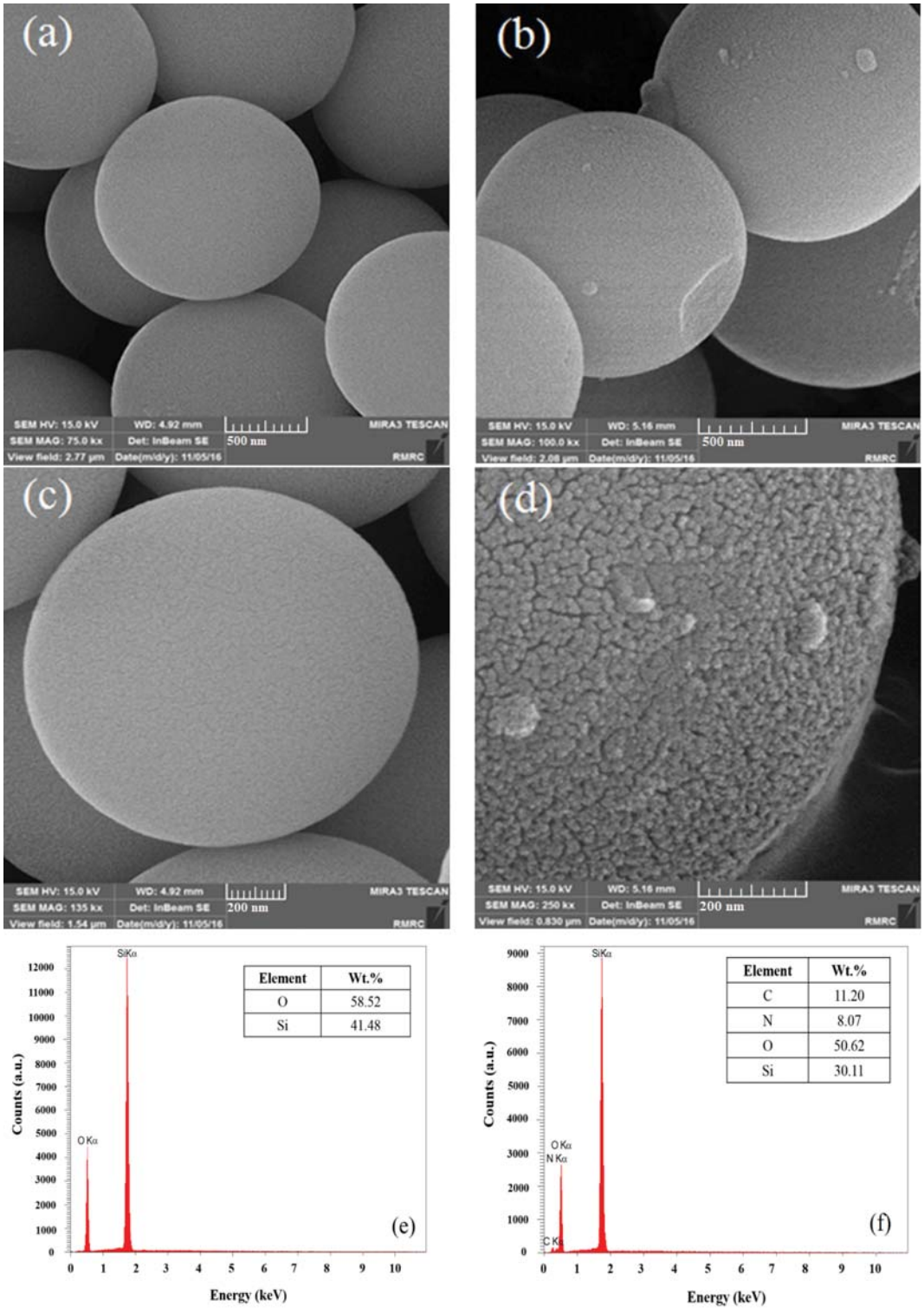

Fig. 2. FESEM images and EDS spectra of ((a), (c), (e)) SM and ((b), (d), (f)) AMSM particles.

respectively, while the peak at 1,085 cm^{-1} is assigned to the asymmetric stretching vibrations of Si-O-Si [25]. The band at 1,632 cm^{-1} in SM sample is due to the O-H bonds of the chemisorbed water. Generation of a new peak at 1,562 cm^{-1}, assigned to the bending vibration of N-H bonds, and wavenumber shift from 1,632 to 1,638 cm^{-1} in AMSM sample confirms the existence of amino groups on AMSM [24,26].

1-2. Morphology and Elemental Analysis

The morphology and elemental analysis of the prepared samples were characterized by FESEM and EDS spectroscopy. Fig. 2 presents the FESEM images along with the EDS spectra of SM and AMSM samples. It is clearly seen that uniform silica spheroids are formed with diameters of approximately a micrometer. The SM sample has a uniform surface morphology, while the introduction of amine groups on the surface generated surface roughness in AMSM sample, which is evident from Fig. 2(b). In addition, the EDS spectra of the samples confirm the introduction of amine groups on SM. Presence of N and C elements in the EDS spectra of AMSM sample signifies this assertion.

1-3. Size and Textural Characteristics

The particle size, texture and morphology of SiO_2 particles in SM samples was observed with the aid of TEM analysis (Fig. 3). It is clearly seen that solid microspheres with smooth external surfaces were formed. Particle-size measurement revealed a high uniform size population approximately in the range of 900 nm to 1 μm, indicating that the samples have a narrow diameter distribution.

1-4. XRD Analysis

Fig. 4 indicates the small angle XRD patterns of AMSM sample, which exhibits a distinguishable peak at approximately 2θ of 0.769°, attributed to the (100) crystallographic orientation of SiO_2 microspheres [26]. The calculated d spacing of (100) orientation was 1.77 nm with the Panalytical X'pert software measurement procedure.

1-5. N_2 Adsorption-desorption Analysis

The nitrogen adsorption/desorption isotherms of SM and AMSM are illustrated in Fig. 5. As can be seen, the pure SM has a type-IV isotherm with H_3 hysteresis loop, observed primarily over relative pressures range of 0.7 to 1.0, characteristic of mesoporous materials with narrow slit-like pore structure [27,28]. On the other hand, the AMSM sample reveals Type-I isotherm corresponding to microporous materials, revealing the alteration in pore structure of bare SM after functionalization with amine groups [29]. The specific textural characteristics of the samples obtained from BET and BJH models are summarized in Table 1. The values of specific surface area (S_{BET}) encountered a reduction from 593.23 $m^2 g^{-1}$ for SM to 66.987 $m^2 g^{-1}$ for AMSM. In addition, functionalization with amine groups reduced the pore volume, although the average pore diameter did not change. These results show that the pore channel may be gradually occupied by the guest material (amine functional groups). Similar results were reported by Mureseanu et al., in which the pore volume and surface area of SBA-15 encountered

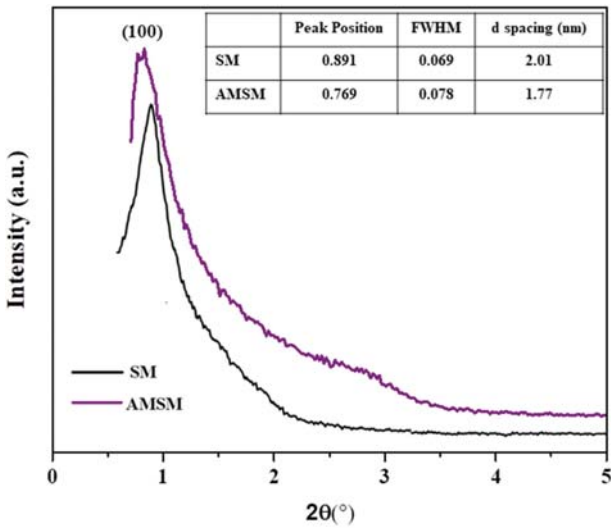

Fig. 4. XRD pattern of AMSM sample.

Table 1. Specific textural characteristics of SM and AMSM obtained from BET and BJH models

Sample	S_{BET} ($m^2 g^{-1}$)	Pore diameter (nm)	Pore volume ($cm^3 g^{-1}$)
SM	593.23	1.21	0.154
AMSM	66.987	1.21	0.0761

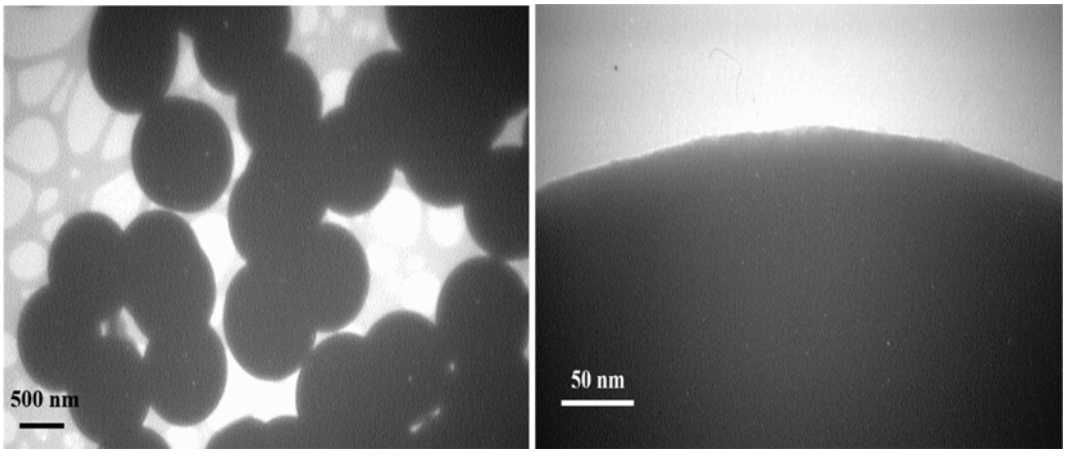

Fig. 3. TEM images of SM sample.

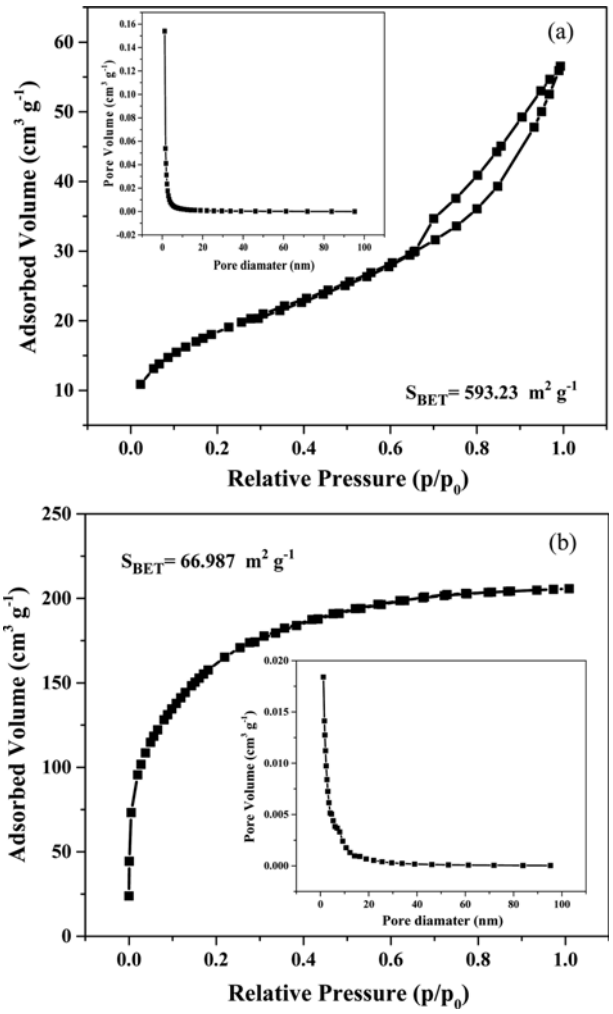

Fig. 5. N_2 adsorption-desorption isotherms and BJH plots of (a) SM and (b) AMSM samples.

a dramatic reduction with aminopropyl functionalization [30].

The amount of amine functional groups on AMSM sample which were generated by TETA treatment can be evaluated based on the results from elemental analysis and value of S_{BET}. The amount of amine groups (mmol) per gram of adsorbent (L_o), the surface density (d) and average intermolecular distance (l) can be calculated using the following equations [31]:

$$L_o = \frac{\text{wt\% of N}}{100 \times \text{atomic mass of N}} \times 1000 \quad (3)$$

$$d = N_a \frac{L_o}{S_{BET}} \quad (4)$$

$$l = \left(\frac{1}{d}\right)^{0.5} \quad (5)$$

where N_a is Avogadro's number. Given the atomic mass of N=14 g mol^{-1}, AMSM contained 5.76 mmol of amine groups per gram of adsorbent, the surface density of d=5.17 groups per nm^2 of adsorbent surface and intermolecular distance of l=0.43 nm, which confirmed that high degree of amine groups were efficiently attached on the surface and pore of the silica microspheres [32].

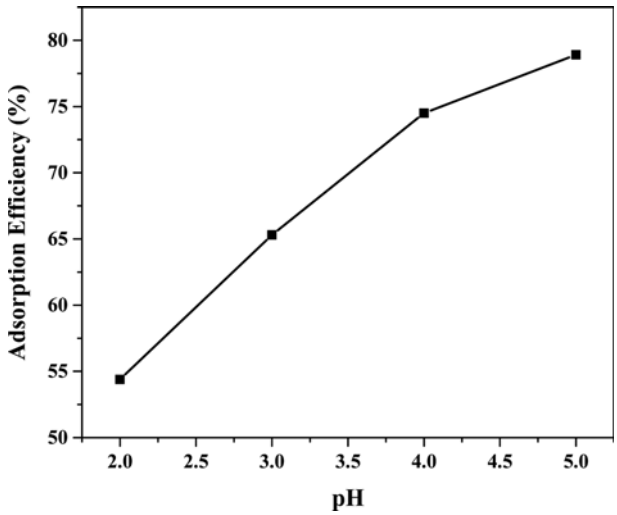

Fig. 6. Effect of pH on adsorption efficiency of AMSM toward Cd(II).

2. Adsorption of Cd(II) Ions

2-1. Optimization of Operational Parameter

2-1-1. Solution pH

The pH of the contaminant solution is considered as one of the most crucial and effective factors in the adsorption of heavy metals because it can both influence the surface charge properties of the adsorbent and the aqueous distribution of metal ions. Therefore, adsorption of Cd(II) ions on the surface of AMSM was studied in the pH range of 2.0 to 5.0 with an adsorbent dosage of 40 mg and initial Cd(II) ion concentration of 50 mg L^{-1} at 298 K. It can be seen in Fig. 6 that the adsorption efficiency encountered a sharp increase from about 45% to 79% when pH was increased from 2 to 5, respectively. It is known that the nitrogen atoms in the structure of amine functional groups are the main adsorption sites on AMSM sample for the removal of heavy metal ions, including Cd(II) due to the presence of lone pair of electrons in nitrogen atoms with the capability of forming metal complexes [33]. However, the pH dependency of amine functional groups covering the surface of SM, which in turn influences the removal efficiency of AMSM for Cd(II), should be taken into account. At lower pH values, the surface of AMSM adsorbent has a positive charge, and therefore lower pH values are not favored for high efficiency adsorption of Cd(II). In addition, the presence of excess H^+ ions in the solution competing with the positive Cd(II) ions is the result of low adsorption efficacy in low pH values (pH=2) [34]. As pH is raised, the number of negatively charged adsorption sites, generated by the deprotonation of amine functional groups on AMSM, increases. Therefore, the high electrostatic attraction between these negatively charged surface of the adsorbent and positively charged Cd(II) ions enhances the adsorption efficiency [35]. Consequently, an initial pH value of 5.0 is considered suitable for the effective removal of Cd(II) ions by the AMSM adsorbent.

2-1-2. Adsorption Time

The required time for an adsorbent to be in contact with the pollutant and become totally saturated is crucial; therefore, it is imperative to study the effect of contact time on the adsorption per-

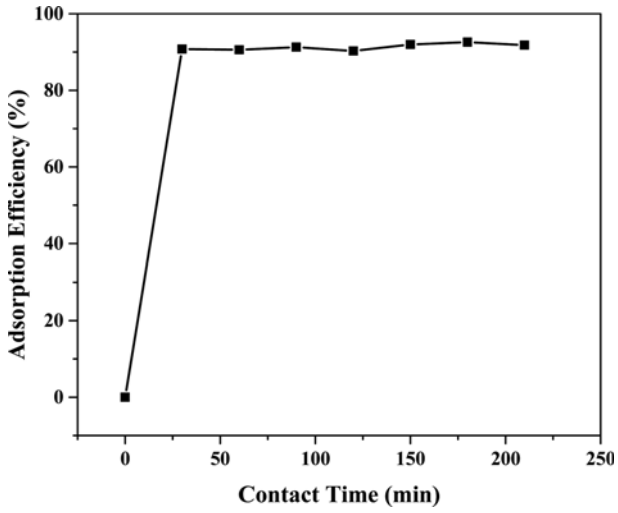

Fig. 7. Adsorption efficiency of AMSM for Cd(II) removal as a function of contact time.

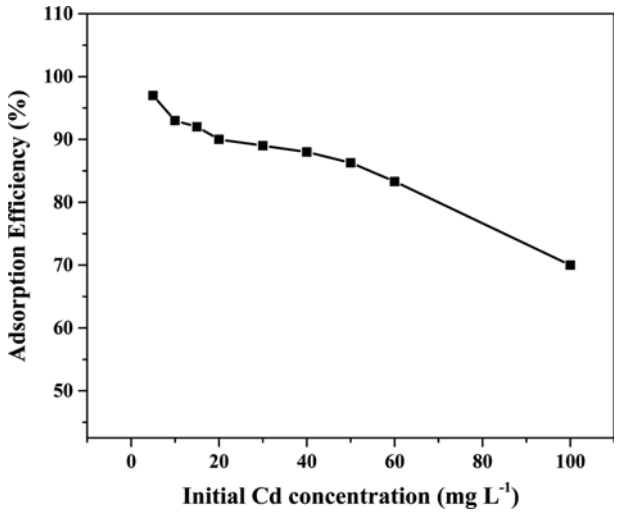

Fig. 9. Adsorption efficiency of AMSM in terms of Cd(II) initial concentration.

formance of the adsorbent for the separation of Cd(II) ions. The effect of adsorption time on the efficiency of Cd(II) is depicted in Fig. 7. The highest separation efficiency was achieved within the initial 30 min and remained almost constant until reaching equilibrium. This is because at the beginning, all the active sites (surface functional groups) were free for adsorbing ions and their concentration decreased gradually as adsorption proceeded with time. The fast uptake rates of Cd(II) ions with AMSM adsorbent represent the high amino loading on the surface of the AMSM because of the coordination between the nitrogen atoms in the amino groups and Cd(II) metal ions, in which lone pair electrons and unoccupied orbits are provided by the nitrogen atoms in the amino groups and the heavy metal ions, respectively [25]. However, to ensure that complete equilibrium is attained throughout the experiments, 150 min shaking period was considered as the optimum agitation period.

2-1-3. Adsorbent Dosage

The variation of adsorption efficiency with the amount of AMSM adsorbent is illustrated in Fig. 8. The adsorption efficiency of AMSM encountered a dramatic rise as the adsorbent dosage was increased from 5 to almost 30 mg, followed by comparably smaller variations toward higher adsorption efficiencies with the dosage changed from 30 to 60 mg. The initial significant enhancement in adsorption efficiency can be due to the high accessibility of larger number of adsorption sites in the initial moments of the adsorption which were progressively occupied with Cd(II) ions. However, the possible aggregation of adsorption sites and an increase in diffusion path length may be the reason for the lower rate increase of adsorption efficiency at higher doses of AMSM. Based on the experiment on the effect of adsorbent dosage, an optimum content of 40 mg was chosen for further investigations.

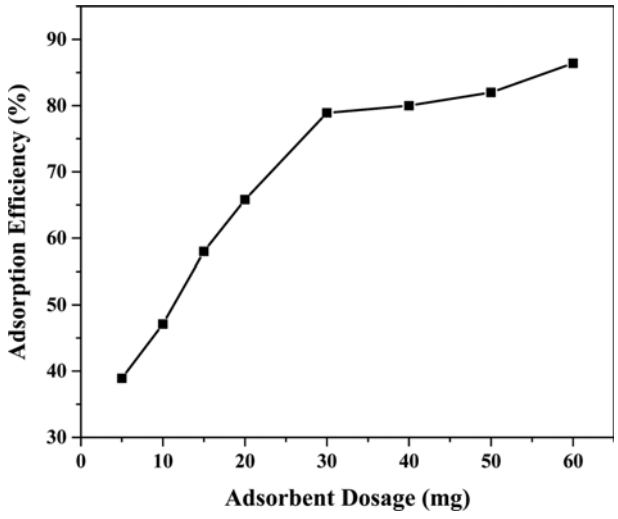

Fig. 8. Effect of adsorbent dosage on adsorption efficiency of AMSM.

2-1-4. Initial Cd(II) Concentration

The adsorption efficiency of AMSM as a function of initial Cd(II) concentration was evaluated from 5 to 100 mg L^{-1}, pH value of 5 and contact time of 150 min. As can be seen in Fig. 9, cadmium removal efficiency decreased from 97.01% to 70.06% by increasing initial cadmium concentration from 5 to 100 mg L^{-1}. At low initial concentrations, Cd(II) ions could easily bind to the free adsorption sites on the surface of AMSM; however, as the initial concentration of metal ions was increased, the number of Cd(II) ions in the solution also increased for the same number of adsorption sites, and therefore the mass transfer driving force and consequently the adsorption efficiency was reduced [36,37].

2-2. Adsorption Isotherms

Important information on adsorption mechanism, surface properties of the adsorbent and adsorbent-adsorbate interactions is provided by the parameters obtained from different isotherm models. Four isotherm models were tested in the present study: Langmuir, Freundlich, Sips and Temkin models, which are defined as follows:

2-2-1. Langmuir Isotherm

The Langmuir isotherm [38] is one the most widely used models applied for the adsorption of pollutants on surfaces. The following equation is the non-linear mathematical representation of the Langmuir isotherm:

$$q_e = \frac{q_{max} K_L C_e}{1 + K_L C_e} \quad (6)$$

where q_e is the adsorption capacity of the adsorbent (mg g^{-1}), C_e is the equilibrium concentration of Cd(II) ions in the solution (mg L^{-1}), q_{max} is the maximum adsorption capacity of the adsorbent (mg g^{-1}), and K_L is the Langmuir isotherm constant (L mg^{-1}). The affinity of the adsorbent toward the adsorbate can be predicted using the essential feature of Langmuir adsorption isotherm parameter (K_L) with the aid of a dimensionless constant called separation factor (R_L):

$$R_L = \frac{1}{1 + K_L C_0} \quad (7)$$

The value of R_L indicates the nature of adsorption to be irreversible (R_L=0), linear (R_L=1) unfavorable (R_L>1), or favorable (0<R_L<1) [39].

2-2-2. Freundlich Isotherm

The Freundlich isotherm [40] is an empirical equation applied to describe the adsorption of pollutants on a heterogeneous surface with a non-uniform distribution of heat of sorption over the surface, generally represented by the following equation:

$$q_e = K_F C_e^{1/n_f} \quad (8)$$

where K_F ((mg g^{-1}) (L $mg^{-1})^{1/n}$) and 1/n are Freundlich isotherm constants related to the adsorption capacity and heterogeneity factor (or adsorption energy), respectively.

2-2-3. Sips Isotherm

The Sips adsorption isotherm [41] is a combination of Freundlich and Langmuir isotherms commonly applied to take into account the effects of indirect adsorbent/adsorbate interactions on adsorption and variation of heat of adsorption with coverage. The Sips isotherm is written as:

$$q_e = \frac{q_s (K_s C_e)^{1/n_s}}{1 + (K_s C_e)^{1/n_s}} \quad (9)$$

where K_S is the Sips isotherm constant (L mg^{-1}) and q_s is the maximum adsorption capacity (mg g^{-1}).

2-2-4. Temkin Isotherm

The Temkin isotherm [42] assumes a uniform distribution of binding energies in adsorption sites for which heat of adsorption reduces with surface coverage, represented by the following equation:

$$q_e = B_T \, Ln(K_T C_e) \quad (10)$$

where K_T is the Temkin isotherm constant (Lg^{-1}), T (K) is the absolute temperature, R the universal gas constant, 8.314 J $mol^{-1}K^{-1}$ and B_T=RT/b is a constant related to the heat of sorption (J mol^{-1}).

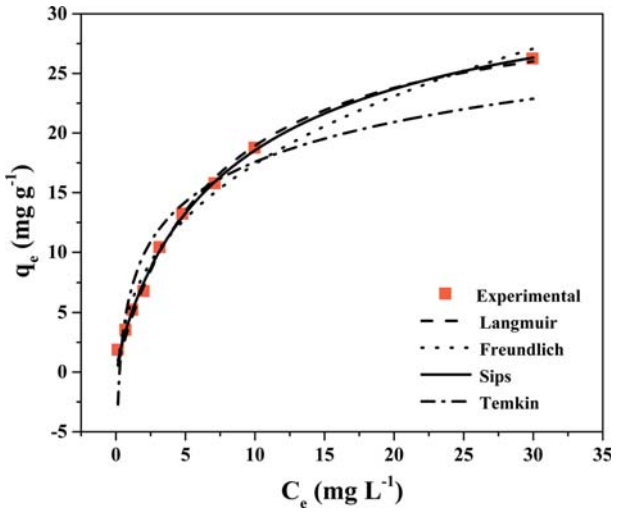

Fig. 10. Langmuir, Freundlich, Sips and Temkin adsorption isotherms for Cd(II) removal on AMSM.

In equilibrium modeling, the precision of the non-linear fitting of the experimental data with isotherm models is analyzed using a non-linear Chi-square (χ^2) test [43]:

$$\chi^2 = \sum_{i=1}^{m} \frac{(q_{e,exp} - q_{e,cal})^2}{q_{e,exp}} \quad (11)$$

Fig. 10 illustrates the non-linear plots of Langmuir, Freundlich, Sips and Temkin adsorption isotherms fitted to the data of Cd(II) removal on AMSM adsorbent for solution pH, amounts of adsorbent and adsorption adjusted at 5.0, 0.375 gL^{-1}, and 150 min, respectively. Isotherm parameters accompanied by the accuracy of each model are represented in Table 2. Based on the values of correlation coefficient (R^2) obtained from the four applied models, the Langmuir and Sips adsorption models had higher consistency in describing the adsorption of Cd(II) ions on AMSM. In this case the comparison of χ^2 values would be beneficial; according to the obtained χ^2 values, it is evident that Sips isotherm model with lower χ^2 (0.247) was the best model to fit Cd(II) adsorption on AMSM. The value of maximum adsorption capacity in this model was calculated as 35.6 mg g^{-1}.

As mentioned, the Temkin adsorption isotherm is commonly applied to account for the possible interactions of adsorbent and adsorbate interactions and the variation of heat of adsorption; the value of B_T obtained from this model can provide information on the physical or chemical nature of adsorption process. In this regard,

Table 2. Isotherm model parameters for adsorption of Cd(II) on AMSM

Langmuir		Freundlich		Sips		Temkin	
K_L (L mg^{-1})	0.145	K_F (L mg^{-1})	5.942	q_s (mg g^{-1})	35.606	K_T (L mg^{-1})	3.80
q_{max} (mg g^{-1})	31.98	$1/n_f$	0.452	K_s (L mg^{-1})	0.110	B_T	4.829
R_L	0.873	n_f	2.212	$1/n_s$	0.872	R^2	0.883
R^2	**0.994**	R^2	0.965	R^2	**0.996**	χ^2	7.443
χ^2	0.364	χ^2	1.447	χ^2	**0.247**		

physisorption processes are reported to have B_T values lower than 20 kJ mol^{-1} [35]. The obtained values for Cd(II) adsorption on AMSM (B_T=4.829) demonstrates that physical interactions were mainly involved.

2-3. Adsorption Kinetics

The mechanism of Cd(II) adsorption and the rate controlling steps were assessed using different linearized kinetic models including:

Pseudo first-order:

$$\ln(q_e - q_t) = \ln q_e - k_1 t \quad (12)$$

Pseudo second-order:

$$\frac{t}{q_t} = \frac{1}{q_e^2 k_2} + \frac{t}{q_e} \quad (13)$$

$$h = k_2 q_e^2 \quad (14)$$

Intraparticle diffusion:

$$q_t = k_i t^{0.5} + C \quad (15)$$

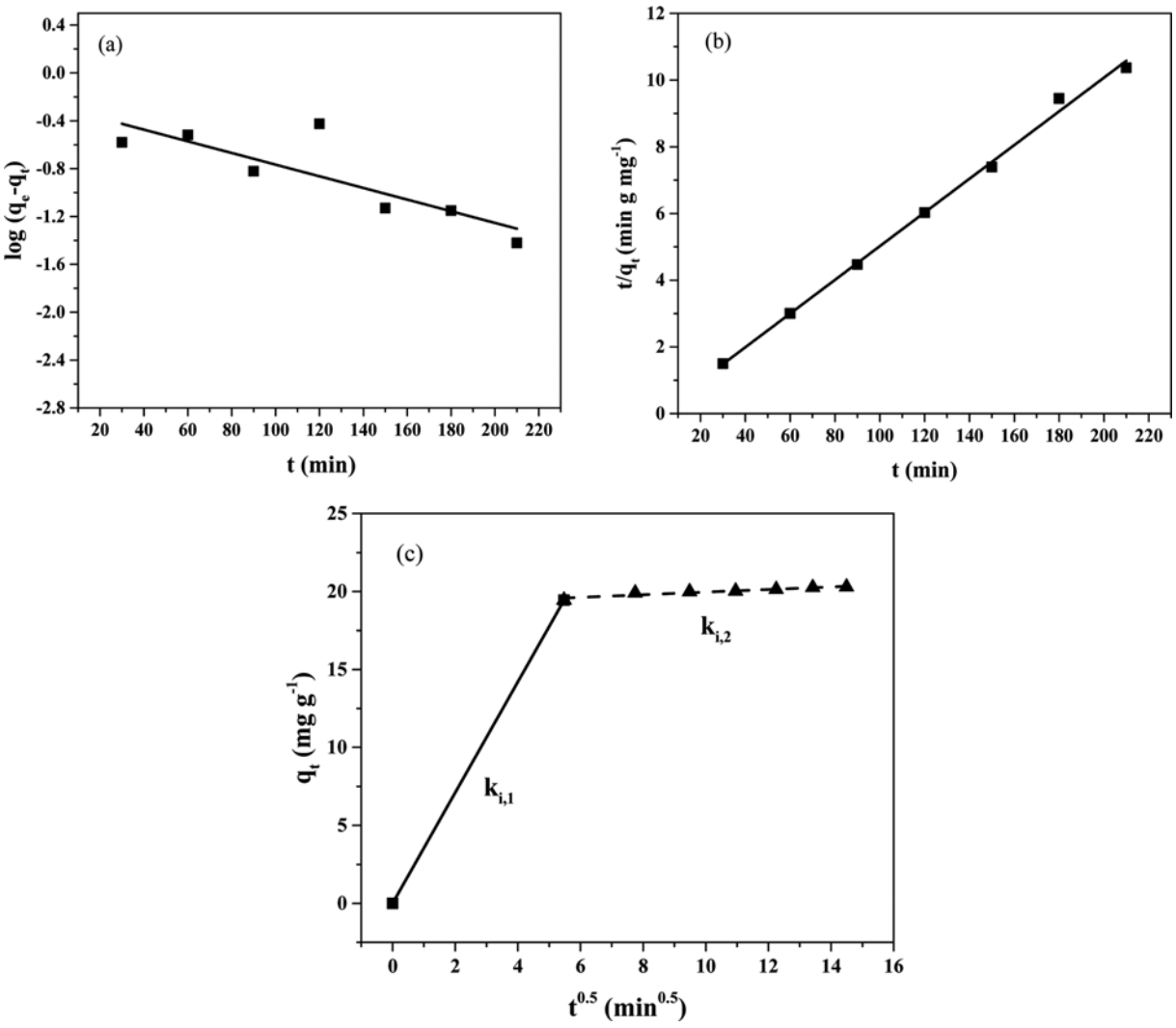

Fig. 11. (a) Pseudo first-order, (b) pseudo second-order and (c) intraparticle diffusion kinetic models for adsorption of Cd(II) on AMSM.

Table 3. Adsorption kinetic rate constants for Cd(II) adsorption on AMSM

Kinetic model	Pseudo first-order		Pseudo second-order		Intraparticle diffusion	
$q_{e,exp}$ (mgg^{-1})	$q_{e,cal}$ (mgg^{-1})	2.312	$q_{e,cal}$ (mgg^{-1})	19.794	$k_{i,1}$ ($gmg^{-1}min^{-0.5}$)	3.551
	k_1 (min^{-1})	0.278	k_2 ($gmg^{-1}min^{-1}$)	0.0794	C_1	1.25e-15
20.287	R^2	0.637	h ($mgg^{-1}min^{-1}$)	31.10	R_1^2	1
			R^2	0.995	$k_{i,2}$ ($gmg^{-1}min^{-0.5}$)	0.0836
					C_2	19.124
					R_2^2	0.987

where q_t is the adsorption capacity at time t (mg g^{-1}), h is the initial adsorption rate (mg g^{-1} min^{-1}), k_1, k_2 and k_i are the rate constants of the pseudo first-order, pseudo second-order and intraparticle diffusion models, respectively, and c is the intraparticle diffusion intercept which gives an idea about the thickness of the boundary layer. The fitted lines and the corresponding kinetic parameters of Cd(II) adsorption on AMSM are shown in Fig. 11 and Table 3, respectively. According to the obtained results, the pseudo-second order equation best fitted the experimental data with higher correlation coefficient (R^2) compared to pseudo-first order equation. To determine the rate controlling step, the intraparticle diffusion model was also used to model the experimental data. According to this model, the plot of q_t versus $t^{0.5}$ should be linear if intraparticle diffusion is involved in the adsorption process and if the corresponding line passes through the origin then intraparticle diffusion is the only rate controlling step [44]. According to Fig. 11(c), it is clear that the plot is multilinear, which indicates that boundary layer effect is also playing a part in the rate of Cd(II) adsorption.

Generally, the kinetics of adsorption is described via three consecutive steps, including external surface diffusion, intraparticle diffusion, and internal diffusion, i.e., the final equilibrium state; these processes may simultaneously affect the rate of adsorption process. In case of Cd(II) adsorption on AMSM, the relatively large value of C_2 demonstrates that a large extent of adsorption was taking place via exterior surface diffusion via amine functional groups on the surface of mesoporous silica spheres. The comparison of rate constant in this model can also simplify the interpretation of adsorption from the kinetic point of view. The lower values of $k_{i,2}$ indicate that although the first initial exterior surface diffusion is responsible for most of the uptake value, the intraparticle diffusion of Cd(II) ions in the highly porous structure of AMSM was the rate controlling step. In fact, as the surface of AMSM becomes saturated (saturation of amine functional groups), Cd(II) ions are forced to diffuse through the internal pore to reach the final equilibrium stage, which is comparatively slower than the initial exterior diffusion process.

2-4. Adsorption Thermodynamics

Thermodynamics of adsorption provide great information about the feasibility and spontaneity of the adsorption process. Standard Gibbs free energy ΔG^o (kJ mol^{-1}), standard enthalpy ΔH^o (kJ mol^{-1}) and standard entropy ΔS^o (J mol^{-1} K^{-1}) are calculated by:

$$K_0 = \frac{q_e}{C_e} \tag{16}$$

$$\Delta G^0 = -RT\ln K_0 \tag{17}$$

$$\ln K_0 = \frac{\Delta S^0}{R} - \frac{\Delta H^0}{RT} \tag{18}$$

The effect of temperature on the adsorption efficiency of AMMS for Cd(II) removal and the van't Hoff plot are depicted in Fig. 12. The calculated values of K_0, ΔG^0, ΔH^0 and ΔS^0 are summarized in Table 4. Increasing temperature leads to lower adsorption capacity and lower values of $\ln K_0$ which is attributed to the exothermic nature of adsorption with adsorption being favored at lower operational temperatures. Negative values of ΔG^0 which reduced as the temperature was increased indicated that the adsorption process

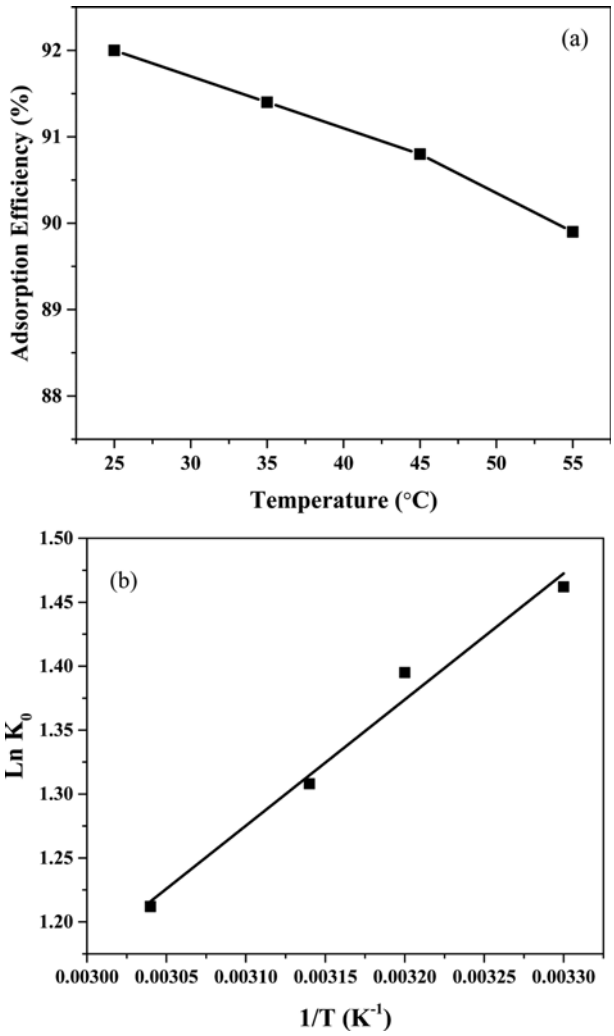

Fig. 12. (a) Effect of temperature and (b) Van't Hoff plot of Cd(II) adsorption on AMSM.

Table 4. Thermodynamic parameters for adsorption of Cd(II) on AMSM

Temperature (K)	$\ln K_0$	ΔG^0 (kJ mol^{-1})	ΔH^0 (kJ mol^{-1})	ΔS^0 (J $mol^{-1}K^{-1}$)
298	1.462	−3.622	−8.199	−14.81
308	1.395	−3.572		
318	1.308	−3.458		
328	1.212	−3.305		

was feasible and spontaneous. The value of ΔG^0 can be used as a measure to determine whether physical or chemical interactions were dominant in the adsorption, ΔG^0 values of 0-20 kJ mol^{-1} are attributed to physisorption involving small energy requirements, while values of 80-400 kJ mol^{-1} are commonly associated with chemical adsorption [45]. The obtained ΔG^0 values evidently indicate that the adsorption of Cd(II) on AMSM adsorbent was mainly through physical interactions, possibly through complexation between amine functional groups and Cd(II) ions or pore diffusion. ΔH^0 and ΔS^0 were obtained from the van't Hoff plot ($\ln K_0$ against

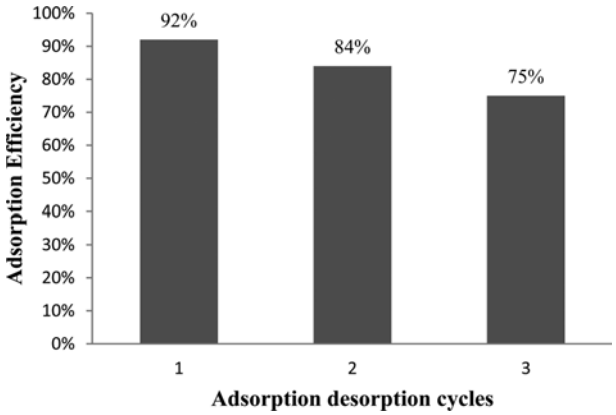

Fig. 13. Consecutive adsorption cycles of Cd(II) adsorption using AMSM.

1/T); the negative values of ΔH^0 correspond to exothermic adsorption of Cd(II) on AMSM, and the negative entropy value indicates decreased randomness at the liquid-solid interface. It is already known that entropy may decrease as a result of energy redistribution between the adsorbate and the adsorbent [46].

2-5. Regeneration

The regeneration capability and versatility of an adsorbent is evaluated by performing sequential adsorption cycles. Fig. 13 depicts the sequential adsorption-desorption cycles of Cd(II) on AMSM. It is obvious that the adsorption efficiency of Cd(II) encountered a reduction from 92% to 75% after three consecutive cycles. This result demonstrates that AMSM adsorbent is a cost-effective adsorbent with an outstanding potential to be recovered and reused in a number of treatment cycles preserving high stability.

CONCLUSIONS

Mesoporous silica microspheres (SM) and amine-functionalized silica microspheres (AMSM) were prepared using a simple chemical method, and the removal ability of AMSM toward Cd(II) ions was further investigated. The products were characterized in terms of chemical structure, morphology and textural properties using Fourier transform infrared spectroscopy (FTIR), X-Ray diffraction (XRD), scanning electron microscopy (SEM), transmission electron microscopy (TEM) and N_2 adsorption-desorption analysis. Both samples were synthesized successfully, without any structural impurities, with a highly porous morphology and comparatively large specific surface area. The average diameter of silica microspheres ranged from 900 nm to 1 μm. The amine functionalized silica microsphere (AMSM) sample was applied as an adsorbent to remove Cd(II) ions from aqueous solution. The effects of operational parameters including pH, contact time, adsorbent dosage, initial concentration of Cd(II) and temperature were evaluated using batch equilibrium experiments. The optimum condition with the highest adsorption capacity was at pH=5, contact time of 150 min, adsorbent dosage of 40 mg, initial Cd(II) concentration of 5 mg L^{-1} and temperature of 298 K. Based on Kinetic studies, the pseudo second-order model provided the highest consistency with the experimental data with intraparticle diffusion being the rate-limiting step of adsorption. Thermodynamic investigations revealed that Cd(II) ions were adsorbed on AMSM through physical interactions. In addition, the Sips isotherm model had the best fit to the equilibrium experimental data with maximum adsorption capacity of 35.606 mg g^{-1}. The obtained results demonstrated that AMSM adsorbent with high adsorption efficiency and fast kinetics can be a suitable adsorbent for the removal of Cd(II) ions from aqueous solution.

REFERENCES

1. M. Ruthiraan, N. M. Mubarak, R. K. Thines, E. C. Abdullah, J. N. Sahu, N. S. Jayakumar and P. Ganesan, *Korean J. Chem. Eng.*, **32**, 446 (2015).
2. M. Yap, N. Mubarak, J. Sahu and E. Abdullah, *J. Ind. Eng. Chem.*, **45**, 287 (2017).
3. K. H. Nelke, M. Mulak, K. Luczak, W. Pawlak, J. Nienartowicz, D. Szumny, M. Kochman and H. Gerber, *Pol. J. Environ. Stud.*, **24**, 1491 (2015).
4. J. Godt, F. Scheidig, C. Grosse-Siestrup, V. Esche, P. Brandenburg, A. Reich and D. A. Groneberg, *J. Occup. Med. Toxicol.*, **1**, 1 (2006).
5. N. Mubarak, M. Ruthiraan, J. Sahu, E. Abdullah, N. Jayakumar, N. Sajuni and J. Tan, *Int. J. Nanosci.*, **12**, 1350044 (2013).
6. E. Da'na, *Micropor. Mesopor. Mater.*, **247**, 145 (2017).
7. D. Purkayastha, U. Mishra and S. Biswas, *J. Water Process Eng.*, **2**, 105 (2014).
8. V. K. Gupta and S. Sharma, *Environ. Sci. Technol.*, **36**, 3612 (2002).
9. H. Ye, Q. Zhu and D. Du, *Bioresour. Technol.*, **101**, 5175 (2010).
10. K. Thines, E. Abdullah, N. Mubarak and M. Ruthiraan, *Renew. Sust. Energy Rev.*, **67**, 257 (2017).
11. T. Sasaki, T. Michihata, Y. Katsuyama, H. Take, S. Nakamura, M. Aburatani, K. Tokuda, T. Koyanagi, H. Taniguchi and T. Enomoto, *J. Agric. Food Chem.*, **61**, 1184 (2013).
12. A. Kundu, B. S. Gupta, M. Hashim, J. Sahu, M. Mujawar and G. Redzwan, *RSC Adv.*, **5**, 35899 (2015).
13. C. Luo, R. Wei, D. Guo, S. Zhang and S. Yan, *Chem. Eng. J.*, **225**, 406 (2013).
14. A. Sari and M. Tuzen, *Appl. Clay Sci.*, **88**, 63 (2014).
15. J. Liang, J. Liu, X. Yuan, H. Dong, G. Zeng, H. Wu, H. Wang, J. Liu, S. Hua and S. Zhang, *Chem. Eng. J.*, **273**, 101 (2015).
16. X. Xue, J. Xu, S. A. Baig and X. Xu, *J. Taiwan Inst. Chem. Eng.*, **59**, 365 (2016).
17. Z. Yu, Q. Dang, C. Liu, D. Cha, H. Zhang, W. Zhu, Q. Zhang and B. Fan, *Carbohydr. Polym.*, **172**, 28 (2017).
18. K. F. Lam, K. L. Yeung and G. McKay, *Environ. Sci. Technol.*, **41**, 3329 (2007).
19. N. Mubarak, R. Alicia, E. Abdullah, J. Sahu, A. A. Haslija and J. Tan, *J. Environ. Chem. Eng.*, **1**, 486 (2013).
20. L. C. Lin, M. Thirumavalavan and J. F. Lee, *CLEAN-Soil, Air, Water.*, **43**, 775 (2015).
21. A. Liu, K. Hidajat, S. Kawi and D. Zhao, *Chem. Commun.*, **1**, 145 (2000).
22. M. Najafi, Y. Yousefi and A. Rafati, *Sep. Purif. Technol.*, **85**, 193 (2012).
23. Y. Le, D. Guo, B. Cheng and J. Yu, *J. Colloid Interface Sci.*, **408**, 173 (2013).

24. J. Jiao, J. Cao, Y. Xia and L. Zhao, *Chem. Eng. J.*, **306**, 9 (2016).
25. S. Hao, A. Verlotta, P. Aprea, F. Pepe, D. Caputo and W. Zhu, *Micropor. Mesopor. Mater.*, **236**, 250 (2016).
26. N. Velikova, Y. Vueva, Y. Ivanova, I. Salvado, M. Fernandes, P. Vassileva, R. Georgieva and A. Detcheva, *J. Non-Cryst. Solids*, **378**, 89 (2013).
27. K. S. Sing, *Pure Appl. Chem.*, **57**, 603 (1985).
28. X. Li, B. Shi, Y. Wang, M. Li, Y. Liu, L. Gao and L. Mao, *Micropor. Mesopor. Mater.*, **214**, 15 (2015).
29. M. Thommes, *Chem. Ing. Tech.*, **82**, 1059 (2010).
30. M. Mureseanu, A. Reiss, I. Stefanescu, E. David, V. Parvulescu, G. Renard and V. Hulea, *Chemosphere*, **73**, 1499 (2008).
31. A. K. Thakur, G. M. Nisola, L. A. Limjuco, K. J. Parohinog, R. E. C. Torrejos, V. K. Shahi and W.-J. Chung, *J. Ind. Eng. Chem.*, **49**, 133 (2017).
32. S. J. Mousavi, M. Parvini and M. Ghorbani, *J. Taiwan Inst. Chem. Eng.*, **84**, 123 (2018).
33. M. Ghorbani and H. Eisazadeh, *Compos. Part B Eng.*, **45**, 1 (2013).
34. M. Pashai Gatabi, H. Milani Moghaddam and M. Ghorbani, *J. Mol. Liq.*, **216**, 117 (2016).
35. M. Pashai Gatabi, H. Milani Moghaddam and M. Ghorbani, *J. Nanopart. Res.*, **18**, 1 (2016).
36. M. Fouladgar, M. Beheshti and H. Sabzyan, *J. Mol. Liq.*, **211**, 1060 (2015).
37. B. Alizadeh, M. Ghorbani and M. A. Salehi, *J. Mol. Liq.*, **220**, 142 (2016).
38. I. Langmuir, *J. Am. Chem. Soc.*, **38**, 2221 (1916).
39. T. W. Weber and R. K. Chakravorti, *AIChE J.*, **20**, 228 (1974).
40. H. Freundlich, *J. Phys. Chem.*, **57**, e470 (1906).
41. O. Redlich and D. L. Peterson, *J. Phys. Chem.*, **63**, 1024 (1959).
42. M. Temkin and V. Pyzhev, *Acta Physiochim. URSS*, **12**, 217 (1940).
43. K. Foo and B. Hameed, *Chem. Eng. J.*, **156**, 2 (2010).
44. M. Xie, L. Zeng, Q. Zhang, Y. Kang, H. Xiao, Y. Peng, X. Chen and J. Luo, *J. Alloys Compd.*, **647**, 892 (2015).
45. T. Sheela and Y. A. Nayaka, *Chem. Eng. J.*, **191**, 123 (2012).
46. M. Rasouli, N. Yaghobi, M. Hafezi and M. Rasouli, *J. Ind. Eng. Chem.*, **18**, 1970 (2012).